Degraded Image Enhancement Using Dual-Domain-Adaptive Wavelet and Improved Fuzzy Transform

Yuehua Huo

China University of Mining and Technology School of Chemical Engineering and Technology: China University of Mining and Technology School of Chemical Engineering

Weiqiang Fan (fan_weiqiang@163.com)

China University of Mining and Technology - Beijing Campus https://orcid.org/0000-0002-4799-5223

Xiaoyu Li

China University of Mining and Technology, Beijing

Research

Keywords: dual-domain, discrete wavelet transform, shrinkage threshold, adaptive adjustment factor, enhancement coefficient, fuzzy enhancement

Posted Date: November 4th, 2020

DOI: https://doi.org/10.21203/rs.3.rs-100022/v1

Degraded image enhancement using dual-domain-adaptive wavelet and improved fuzzy transform

Yuehua Huo,[1,2] Weiqiang Fan,[1]* and Xiaoyu Li [1]

[1] School of Mechanical Electronic and Information Engineering, China University of Mining and Technology ,Beijing, Beijing 100083, China
[2] Network and Information Center, China University of Mining and Technology, Beijing, Beijing 100083, China.

*Corresponding author. E-mail: fan_weiqiang@163.com

Abstract A novel enhancement algorithm of degraded image based on dual-domain-adaptive wavelet and improved fuzzy transform is proposed, aiming at the problem of surveillance videos degradation caused by complex lighting conditions underground. The dual-domain filtering (DDF) is used to decompose the image into low-frequency sub-image and high-frequency sub-images. The contrast limited adaptive histogram enhancement (CLAHE) is used to adjust the overall brightness and contrast of the low-frequency sub-image. Discrete wavelet transform (DWT) is used to obtain low frequency sub-band (LFS) and high frequency sub-band (HFS). The wavelet shrinkage threshold method based on Bayesian estimation is used to calculate the wavelet threshold corresponding to the HFS at different scales. A Garrate threshold function that introduces adaptive adjustment factor and enhancement coefficient is designed to adaptively de-noise and enhance the HFS coefficients corresponding to wavelet thresholds at different scales. Meanwhile, the gamma function is used to realize the correction of the LFS coefficients. The constructed PAL fuzzy enhancement operator is used to perform contrast enhancement and highlight area suppression on the reconstructed image to obtain an enhanced image. The proposed algorithm is evaluated by subjective vision and objective indicators. The experimental results show that the proposed algorithm can significantly improve the overall brightness and contrast of the original image, suppress noise of dust & spray, enhance the image details and improve the visual effect of the original image. Compared with the images enhanced by the STFE, GTFE, CLAHE, SSR, MSR, DGR, and MSWT algorithms, the comprehensive performance evaluation indicators of the images enhanced by the proposed algorithm are increased by 312.50%, 34.69%, 53.49%, 22.22%, 32.00%, 10.00%, 60.98%, 3.13%, respectively. At the same time, comprehensive performance evaluation indicator of the enhance image and the robustness is the best, which is more suitable for image enhancement in different mine environments.

Keywords dual-domain, discrete wavelet transform, shrinkage threshold, adaptive adjustment factor, enhancement coefficient, fuzzy enhancement

1. Introduction

With the increasing contradiction between mine safety production and economic benefits, related safety issues have attracted wide attention from the country and society (Sun JP 2010; Wang GF et al. 2019). Coal mine underground video monitoring system and video intelligent analysis system are important means to grasp the location and status of underground personnel, equipment, vehicles and other moving targets (Xu ZQ et al. 2020; Zhang F et al. 2018; Zhang W

et al. 2018). However, the images of surveillance videos are susceptible to coal mine dust & spray, uneven lighting or low illumination of artificial light source and other environments, resulting in poor image quality captured by the camera (Han H et al. 2020; Zhi N et al. 2017). This directly affects the mine dispatch center's accurate control of the actual underground situation and subsequent data analysis. Therefore, in order to better present the scene information of coal mine, highlight the overall and edge features of the image, improve the visual effect of the image, and promote the application of the underground video monitoring system in the coal mine safety production and intelligent analysis, it is of great significance to study the image enhancement of the coal mine video.

At present, some scholars at home and abroad have only studied the image enhancement under uneven illumination or low illumination conditions, but there are few reports on video image enhancement under complex lighting conditions in coal mines. As described in Zhi N et al. (2017), Si L et al. (2017), and Wang DW et al. (2018), the mine uneven light image enhancement based on retinex algorithm is realized. The "S-type" function is set to adjust the contrast of the image to achieve image enhancement, but nonlinear distortion exists in this method, which results in blurred edge features. Meanwhile, this kind of algorithm has the following shortcomings: ①The traditional filter estimates irradiation component (LC), which is easy to cause the edge feature of the enhanced image to be blurred; ② The edge preservation filter estimates LC, but the enhancement process takes a long time; ③The algorithm needs to assume that the ambient light is uniform, which is not suitable for artificial light source scene under the mine. Discrete wavelet transform (DWT) is an important method of image enhancement, which has better time-frequency local characteristics and multi-resolution analysis characteristics Hu K et al. (2020) and Juneja S et al. (2018) proposed image enhancement methods using DWT and SVD, applying SVD to DWT's low frequency sub-band (LFS) coefficients, and using inverse DWT to reconstruct the processed high frequency sub-band (HFS) coefficients and LFS coefficients. The improvement effect is good, but the brightness and SNR of the enhanced image are small. The DWT transform domain based gamma correction proposed in Kallel F et al. (2017) and Zhou M et al. (2018) have an obvious enhancement effect on degraded images under complex lighting conditions. However, the wavelet threshold function adopted is likely to lead to the loss of image details or the improvement of contrast is not obvious, and the process of manually adjusting required gamma value is tedious. Singh H (2018) proposed a piecewise gamma-corrected histogram equalization framework using PSO by analyzing the advantages and disadvantages of histogram and gamma transformation. This algorithm has a better enhancement effect on degraded images of mines, but the parametric iterative optimization process of PSO takes a long time, and easy to fall into the local optimal solution.

In this paper, a Garrate threshold function that introduces adaptive adjustment factors and enhancement coefficients and an improved PAL fuzzy transform function are designed. At the same time, it combines the advantages of DDF, CLAHE, DWT and gamma transform, and proposes an enhancement algorithm of degraded image using dual-domain adaptive wavelet and fuzzy transform. First, the input image is decomposed into low-frequency sub-images representing the approximate information of the original image and high-frequency sub-images of detailed information through DDF. Secondly, the CLAHE is used to adjust the brightness and contrast of the low-frequency sub-images. Then, a Garrate threshold function

including adaptive adjustment factor and enhancement coefficient is used to adaptively de-noise and enhance the HFS coefficients of the high-frequency sub-image, and the HFS coefficients of the de-noising and enhanced are adjusted by using gamma transformation; Finally, the improved PAL fuzzy transformation method is used to suppress the halo and adjust the highlight area of the reconstructed image, and then the enhanced image is obtained. The rest of the paper is organized as follows. The basic principle of the proposed algorithm model is described in Section 2. The algorithm realization process is described in Section 3. The experimental results and analysis are discussed in Section 4. Some conclusions are summarized in Section 5.

2. Image Enhancement Algorithm Modeling

The DWT can transform the image from spatial domain to frequency domain, without losing the original information of the image, and increasing redundant information (Karan SK et al. 2018). Meanwhile, it has perfect reconstruction ability (Yang CC et al. 2018; Bae C, et al. 2017). However, the existing two-dimensional wavelet threshold function and threshold selection model have limited application scope. In complex lighting scenes in mines, traditional wavelet enhancement algorithms are easy to lose image detail features in HFS or amplify image noise, and meanwhile, unprocessed or poorly processed LFS coefficients containing image outline features. As a result, images of wavelet reconstruction (WR) appear blurred to varying degrees. Therefore, it is necessary to design an image enhancement model that meets the complex lighting conditions of the mine.

2.1 Wavelet enhancement model design

The construction of wavelet threshold function is the key to the design of enhancement model. At present, the image enhancement algorithm using wavelet transform mainly uses traditional wavelet hard threshold function, soft threshold function (Lei S et al. 2020; Vishwakarma A et al. 2018), and improved wavelet threshold function models: Semisoft threshold function (Zhang LX et al. 2018) and Garrote threshold function (Il KK et al. 2017). According to the defects of the four typical wavelet threshold functions in different degrees (He F et al. 2019) and the characteristics that the noise signal in HFS decreases gradually with the increase of Wavelet decomposition (WD) scale. a Garrote threshold function including adaptive factor is designed (as shown in Fig.1. This function is defined as in Eq. (1):

$$H\ \omega_{i,j}\ =\begin{cases}\operatorname{sgn}\ \omega_{i,j}\ \dfrac{1-s_i}{T_i}\omega_{i,j}{}^{2}\ , & \left|\omega_{i,j}\right|<T_i\\ \omega_{i,j}-s_i\dfrac{T_i^2}{\omega_{i,j}}e^{T_i-\left|\omega_{i,j}\right|}\ , & \left|\omega_{i,j}\right|\geq T_i\end{cases} \tag{1}$$

where H is the HFS coefficient after wavelet de-noising; s_i is an adaptive factor at the ith scale, $s_i \in (0,1)$; $\omega_{i,j}$ is the jth HFS of the ith layer WD, j=1, 2, 3, respectively corresponding to HL, LH, HH sub-bands; $\operatorname{sgn}\cdot$ is a symbolic function; T_i is the wavelet threshold at the ith scale.

In the model, s_i can dynamically adjust according to the distribution of noise coefficients after WD, which greatly improves the flexibility and practicability of the model. s_i is obtained by the following Equation:

$$s_i = m / M \tag{2}$$

where M is the length of the HFS at the ith scale; m is the number of frequencies that the HFS at the ith scale is less than the threshold.

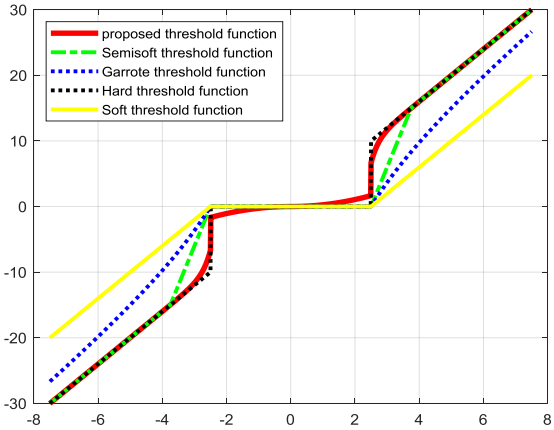

(a)

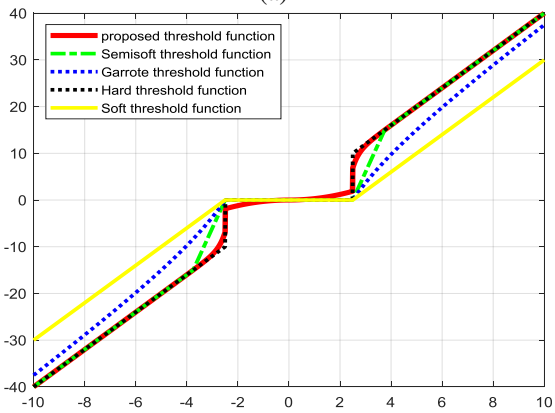

(b)

Fig.1 The proposed threshold function

Generally, the HFS after WD contains not only a large amount of detail information but also some noise information (Singh H et al. 2018). If the wavelet threshold function of Eq.(1) is directly used for image detail information enhancement, the noise signal will also be amplified to the same extent, which will affect the visual effect of the image. Therefore, this paper introduces the adaptive adjustment factor and the adaptive enhancement coefficient that vary with scale to achieve adaptive noise reduction and enhancement of HFS coefficients at different scales. The adaptive wavelet threshold function is:

$$H'(\omega_{i,j}) = \begin{cases} \operatorname{sgn}(\omega_{i,j}) \dfrac{1-s}{T} W_{i,j} \omega_{i,j}^{2}, & |\omega_{i,j}| < T \\ W_{i,j}\omega_{i,j} - s\dfrac{W_{i,j}T^{2}}{\omega_{i,j}} e^{W_{i,j}(T-|\omega_{i,j}|)}, & |\omega_{i,j}| \geq T \end{cases} \tag{3}$$

where H' is the HFS coefficient after wavelet de-noising and enhancement; $W_{i,j}$ is the adaptive enhancement coefficient of the jth HFS under the ith scale.

The scale of WD is negatively correlated with the detailed information in the corresponding HFS (Singh H et al. 2018). Therefore, $W_{i,j}$ can be obtained by Eq. (4):

$$W_{i,j} = ke^{\frac{(\omega_{i,j}-\mu)^{2}}{2\sigma^{2}}} \tag{4}$$

where μ and σ are the mean and standard deviation of the jth HFS under the ith scale, respectively. k is an adaptive adjustment parameter.

After WD, the HH sub-image at the same scale contains more details of the original image, while the HL and LH sub-images have less detailed features and larger approximate features (Saravani S et al. 2018). Therefore, when j=1, 2, k=2i-1; when j=3, k=2i.

According to Eqs. (3) and (4), the adaptive wavelet threshold function designed is continuous and smooth in the whole definition domain, there is no constant deviation. According to the change of WD scale, it can perform adaptive threshold transformation for HFS at each scale, highlight the detailed features of different scales, suppress the noise level of the image, enhance the layering of the image, and greatly improve

the flexibility and practicality of the wavelet threshold function.

2.2 Threshold selection

In image enhancement processing based on DWT, the selection of wavelet threshold is a decisive factor in determining the image enhancement effect. As the scale of WD increases, the noise coefficient in the corresponding HFS will become smaller and smaller (Sha YY et al. 2018). The same threshold is used at different scales, if the threshold is selected too large, the effective wavelet coefficient below the threshold is set to zero, resulting in the blurring of image details and edge features; if the threshold is selected too small, the wavelet coefficients after de-noising still contains a lot of noise, which reduces the de-noising effect of the image enhancement algorithm. Therefore, the paper uses the wavelet shrinkage threshold method based on the Bayesian estimation to achieve adaptive adjustment of the wavelet threshold. The specific calculation process is as follows:

1） According to the Bayesian estimation theory (Chetih N et al. 2017), each HFS coefficient after wavelet de-noising obeys a generalized Gaussian distribution with a mean of 0 and a variance of σ_x^2.

$$\Phi\ x\ = \frac{1}{\sqrt{2\pi\sigma_x^2}} \exp\left(-\frac{x^2}{2\sigma_x^2} \right) \tag{5}$$

where x and σ_x are the jth HFS coefficient and standard deviation at the ith scale.

2） When the parameter σ_x is given, the optimal threshold T can be found according to the Bayesian risk estimation function $r\ T$ (Sachin DR et al. 2012). According to the threshold calculation Equation in Tang P et al. (2017):

$$T_i = \frac{\sigma^2}{\sigma_x} \tag{6}$$

where T_i is the threshold of the HFS coefficient of the ith scale; σ^2 is the noise variance of the jth HFS coefficient of the ith layer. In noise estimation, usually j=3.

3） The noise variance is calculated using the robust median estimation Eq.(7):

$$\sigma = \text{median}\ \left| \omega_{i,j} \right| \ / 0.6745 \tag{7}$$

4） The variance estimate of each noisy observation sub-band is obtained by the maximum likelihood estimation method:

$$\sigma_y^2 = \frac{1}{n} \sum_{x=1}^{n} \omega_{i,3}^2 \ \ x \tag{8}$$

where n is the length of the HH sub-band under the ith layer.

5）Obtained by $\sigma_y^2 = \sigma_x^2 + \sigma^2$:

$$\sigma_x = \sqrt{\max\ \sigma_y^2 - \sigma^2, 0} \tag{9}$$

The adaptive wavelet threshold T at different wavelet scales is calculated by using Eqs. (6) - (9).

2.3 Gamma transform

The low brightness of the mine degraded image is easy to cause the LFS coefficients after WD to be small as a whole, which makes the image contour characteristics after WR not obvious. Therefore, in this paper, the Gamma transform is used to correct LFS coefficients, highlight the contour characteristics of the reconstructed image and improve the overall brightness of the degraded image. Gamma transform by using Eq.(10) (Zhuang LY et al. 2019).

$$f_{\mathrm{LFS}}(x,y)=\left(\frac{f_{\mathrm{LFS}}(x,y)-f_{\mathrm{LFS,min}}(x,y)}{f_{\mathrm{LFS,max}}(x,y)-f_{\mathrm{LFS,min}}(x,y)}\right)^{1/\varepsilon} * \left(f_{\mathrm{LFS,max}}(x,y)-f_{\mathrm{LFS,min}}(x,y)+f_{\mathrm{LFS,min}}(x,y)\right) \quad (10)$$

where $f_{\mathrm{LFS}}(x,y)$ is the LFS coefficients after gamma transformation; $f_{\mathrm{LFS}}(x,y)$ is the LFS coefficients; $f_{\mathrm{LFS,max}}(x,y)$ is the maximum value of the LFS coefficients; $f_{\mathrm{LFS,min}}(x,y)$ is the minimum value of the LFS coefficients; ε is an adjustable parameter, which is used to control the degree of enhancement or suppression of image brightness.

In general, the larger ε, the greater the degree of enhancement, the more obvious the brightness increase. The smaller ε, the greater the degree of suppression, the more obvious the brightness suppression. The brightness of the mine degraded image is overall dark, and only part of the area has higher brightness. Therefore, generally in mine image enhancement, $\varepsilon = 2.5$.

2.4 Improved PAL fuzzy enhancement algorithm

After image reconstruction, the brightness and contrast of mine degraded images have been improved to a certain extent, but the effect of suppressing the image halo caused by artificial light sources is not obvious. In order to further enhance the detailed features of the degraded image and suppress its image halo, an improved PAL fuzzy enhancement algorithm is designed to achieve blur enhancement of the reconstructed image. The specific steps are as follows:

1）Design a membership function:

$$Y_{m,n}=\frac{X_{m,n}-X_{\min}}{D\,(X_{\max}-X_{\min})},\quad 1\le D\le 2 \quad (11)$$

where $X_{\max}=\max\{X_{m,n}\}$ and $X_{\min}=\min\{X_{m,n}\}$ are the maximum and minimum values of all pixels in the image after WR; D is the control parameter, $D\in[1,2]$.

2）Calculate the membership of the elements in the reconstructed image by using Eq.(11), and perform the fuzzy operation through the constructed fuzzy enhancement operator. Fuzzy enhancement operator:

$$Y'_{m,n}=\begin{cases}2Y_{m,n}^{1/2}, & 0\le Y_{m,n}<0.5\\ 2Y_{m,n}^{2}-Y_{m,n}+1, & Y_{m,n}\ge 0.5\end{cases} \quad (12)$$

3）Inverse fuzzy transformation is performed on the fuzzy enhancement coefficient obtained by using Eq.(12). Anti-fuzzy transform function:

$$f_{\mathrm{E}}=D\,(X_{\max}-X_{\min})\,\frac{Y'_{m,n}}{2}+X_{\min} \quad (13)$$

The improved PAL fuzzy enhancement algorithm uses a membership function containing control parameters D to transform the image from the spatial domain to the fuzzy set domain. According to the designed fuzzy enhancement operator, the image halo suppression and the low illumination area enhancement are performed, and the final enhanced image is obtained by the anti-fuzzy transformation function. By adjusting the value of D, the membership of the gray values of different degraded images is controlled, and then the video surveillance images in different lighting areas of the mine are enhanced, which greatly improves the robustness of the proposed algorithm.

3. Implementation Process of the Proposed Algorithm

The paper proposes the enhancement algorithm of degraded image based on dual-domain-adaptive wavelet and improved fuzzy transformation. The specific implementation steps can be shown as follows:

Step 1: Perform DDF (Fan WQ et al. 2020) on the 3-channel of the original image f (i.e., R, G, B) to obtain the low-frequency sub-image and high-frequency sub-images of the three channels respectively.

Step 2: CLAHE algorithm is used to adjust the illumination and contrast of the acquired 3-channel low-frequency sub-images.

Step 3: Use the "db5" wavelet base (Sun HD et al. 2014) to perform 3-layer WD on the high frequency sub-images to obtain LFS and HFS at each scale.

Step 4: Calculate the wavelet threshold T and adaptive weighting factor s corresponding to each scale HFS.

Step 5: Calculate the adaptive enhancement coefficient $W_{i,j}$ for each scale HFS according to Eq.(4).

Step 6: The adaptive weight factor s, adaptive enhancement coefficient $W_{i,j}$ and wavelet threshold T are introduced into the adaptive wavelet threshold function of Eq.(3) to achieve de-noising and enhancement of HFS at various scales.

Step 7: The LFS coefficients after WD are gamma-transformed, and WR is performed on each scale HFS after de-noising & enhancement and the LFS after gamma transformation.

Step 8: Repeat the above steps 3 ~ 7 to obtain the 3-channel high-frequency sub-images after WR.

Step 9: Reconstruct the processed 3-channel low-frequency sub-image and the 3-channel high-frequency sub-image after WR to obtain a reconstructed image.

Step 10: Convert the reconstructed image from the RGB color model to the HSV color model, and use the improved PAL fuzzy enhancement algorithm to blur the acquired V channel image, and obtain the final enhanced image.

The block diagram of the proposed algorithm implementation principle is shown in Fig.2.

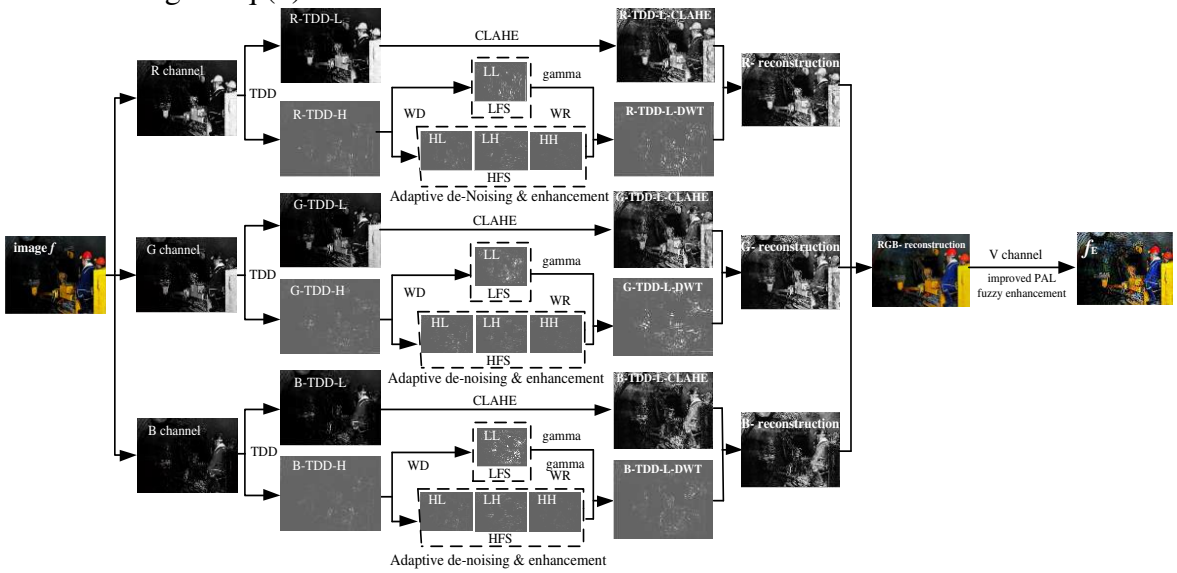

Fig.2 Block diagram of the proposed algorithm implementation principle

4 Experimental and Result Analysis

In order to verify the practical application effect of the proposed algorithm, some degraded images in different mine monitoring videos were selected. Experimental computer configuration: Inter Core i7-10750H CPU, 2.60 GHz, RAM 16GB, programming tool: Matlab R2020a. Analyze the enhanced performance of the proposed algorithm and the other 7 comparison algorithms from two aspects: subjective vision and objective indicators. The 7 comparison algorithms are the Semisoft threshold function enhancement (STFE), the Garrate threshold function enhancement (GTFE), CLAHE (Wang DW et al. 2018), single scale retinex (SSR) (Si L et al. 2017), multi-scale retinex (MSR) (Zotin A et al. 2018), double Gamma retinex (DGR) (Zhi N et al. 2018), contrast limited adaptive histogram equalization discrete wavelet transform (CLAHE-DWT) (Huang LD et al. 2015). Some parameter settings in the above comparison algorithm: the STFE and the GTFE use fixed threshold (sqtwolog), the enhancement coefficient $W_{i,j}$=2, other parameters are the same as the algorithm proposed. CLAHE uses the default parameters, and SSR uses Gaussian filter. MSR uses the default parameters of multi-resolution McCann. DGR and CLAHE-DWT respectively use the parameters recommended in the original reference.

4.1 Subjective visual analysis

1) Experiment 1: The low illumination image with a resolution of 355×568 is enhanced, and the experimental results are shown in Fig.3.

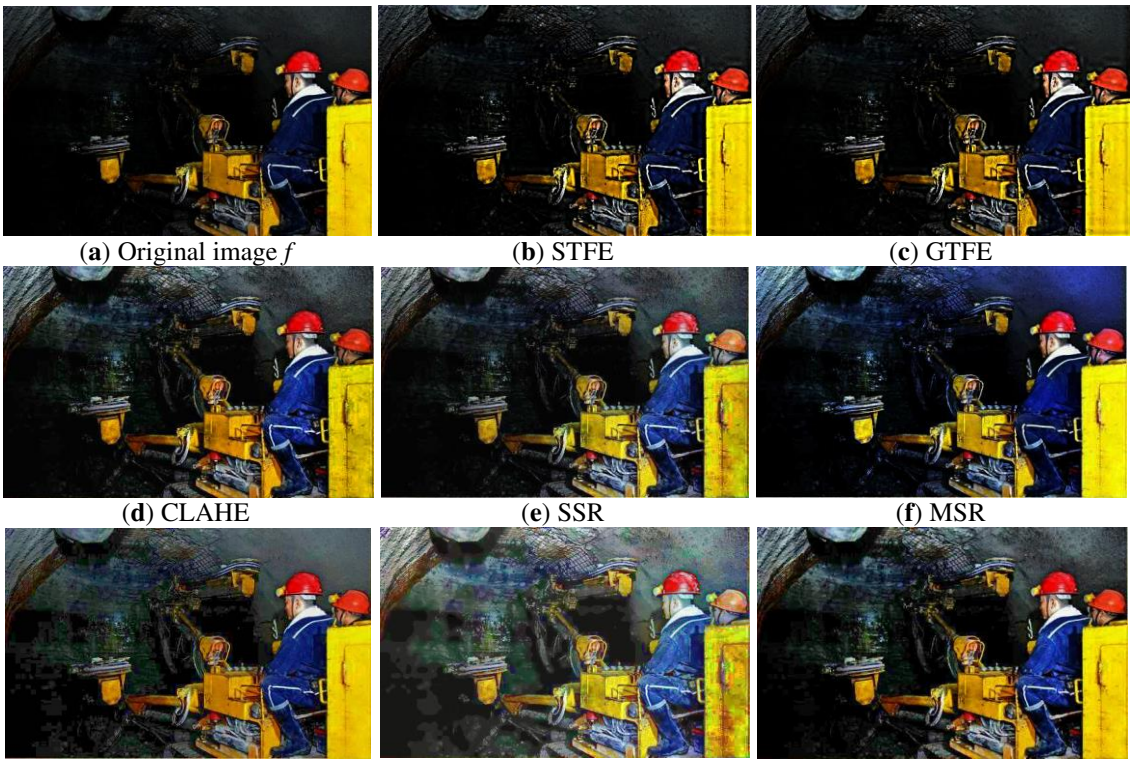

(**a**) Original image *f* (**b**) STFE (**c**) GTFE

(**d**) CLAHE (**e**) SSR (**f**) MSR

(**g**) DGR (**h**) CLAHE-DWT (**i**) Target algorithm

Fig.3 Low illumination image enhancement comparison chart

2) Experiment 2: The dust & spray image with a resolution of 520×920 is enhanced, and the experimental results are shown in Fig.4.

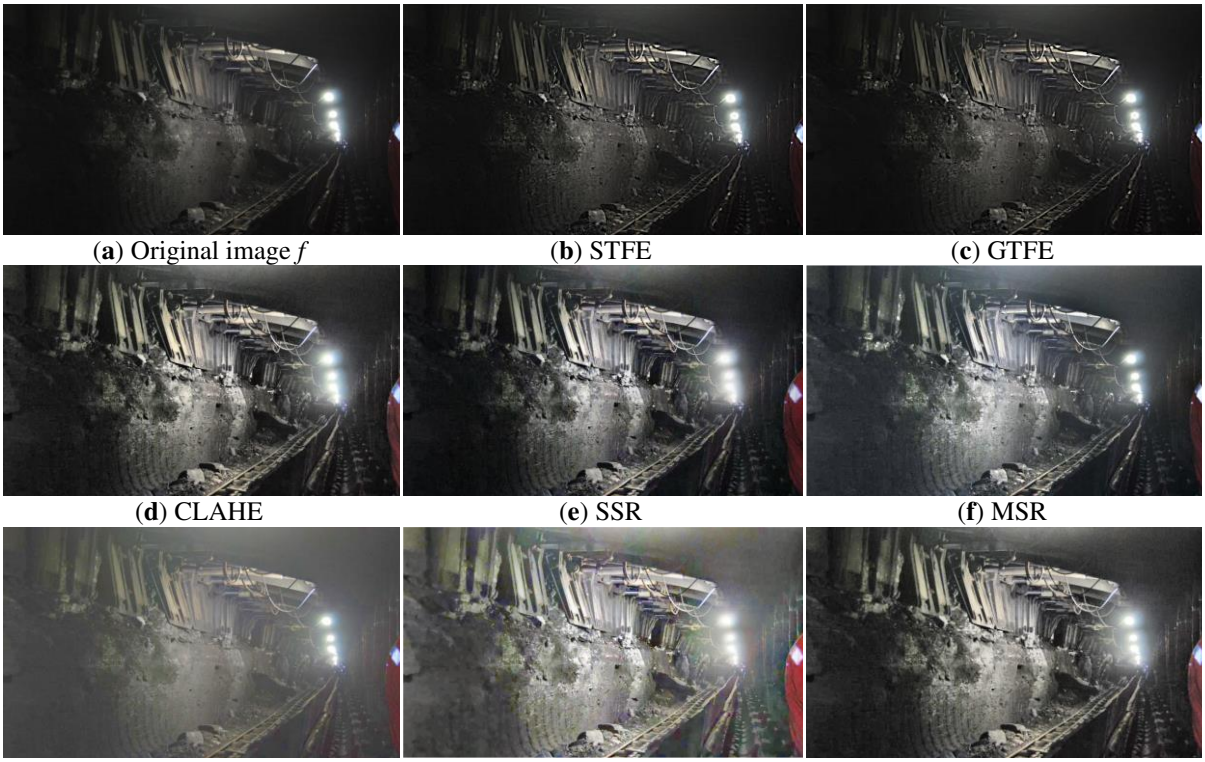

(**a**) Original image *f* (**b**) STFE (**c**) GTFE

(**d**) CLAHE (**e**) SSR (**f**) MSR

(**g**) DGR (**h**) CLAHE-DWT (**i**) Target algorithm

Fig.4 Dust & spray image enhancement comparison chart

3) Experiment 3: The uneven lighting image with a resolution of 520×920 is enhanced, and the experimental results are shown in Fig.5.

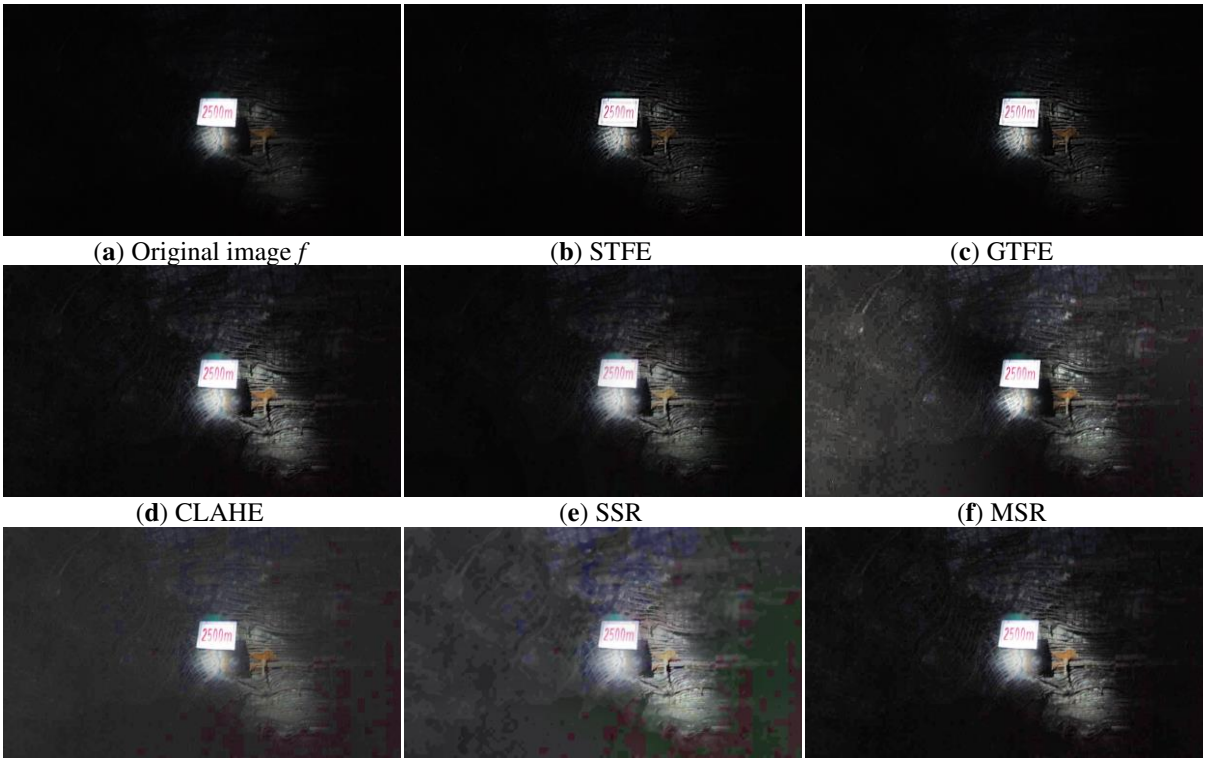

(**a**) Original image *f* (**b**) STFE (**c**) GTFE

(**d**) CLAHE (**e**) SSR (**f**) MSR

(**g**) DGR (**h**) CLAHE-DWT (**i**) Target algorithm

Fig.5 Uneven lighting image enhancement comparison chart

Comparing the original images and the enhanced visual effect images (Fig. 3 - 5), it can be seen that in the original images 3(a) - 5(a), the degraded images of mines

have low brightness and contrast, severe dust & spray interference, and uneven illumination of artificial light sources. The enhancement effects of different algorithms are significantly different. The contrast of images 3(b) - 5(b), 3(c) - 5(c) enhanced by STFE and GTFE is significantly improved, but the brightness and uneven illumination of the image have not been improved. The brightness and contrast of the images 3(d) ~ 5(d) enhanced by the CLAHE are improved to a certain extent, but the edges of the image are prone to halo and blurred edges. Images 3(e) - 5(e) enhanced by SSR have over-enhancement phenomenon. The images 3(f) - 5(f) enhanced by the MSR are better than STFE, GTFE, CLAHE, and SSR, but it also has color distortion. The brightness of the images 3(g) - 5(g) enhanced by the DGR is significantly improved, but the image is easy to edge blur, and seriously distorted in the uneven lighting environment of the mine. The brightness of the images 3(h) - 5(h) enhanced by CLAHE-DWT is obviously improved, but the contrast of the image is reduced and the edges are blurred. In the above three scenarios, the images enhanced by the target algorithm have significant improvements in overall brightness, contrast, color, and edges, and the visual effect is better than the other seven contrast algorithms.

4.2 Objective index analysis

In order to objectively evaluate the effect of image enhancement, the paper adopts Mean (image brightness) (Singh H et al. 2018), mean local mean square error (MLMSE) (image contrast), peak signal to noise ratio (PSNR) (noise suppression level), mean local information entropy (MLIE) (information richness) (Fan WQ et al. 2020), structural similarity indicator (SSIM) (image distortion degree) (Kaur A et al. 2017) 5 indicators for performance evaluation and comparison. The objective indicators data of low illumination (Experiment 1), dust & spray (Experiment 2), and uneven lighting (Experiment 3) underground coal mines are shown in Tables 1 - 3.

Table 1 Evaluation indicator values of enhanced images under low illumination

Evaluation index	Mean	MLMSE	PSNR	MLIE	SSIM
Original image *f*	34.91	226.52	——	2.01	——
STFE	36.67	488.95	26.12	2.02	0.98
GTFE	36.56	476.08	26.29	1.99	0.98
CLAHE	52.26	402.29	19.12	2.15	0.85
SSR	53.88	375.12	18.62	2.16	0.84
MSR	47.23	423.26	21.68	2.09	0.94
DGR	60.89	293.63	17.87	2.10	0.81
CLAHE-DWT	88.52	401.94	11.86	2.18	0.53
Target algorithm	59.15	405.68	17.35	2.25	0.80

Table 2 Evaluation indicator values of enhanced images under dust & spray

Evaluation index	Mean	MLMSE	PSNR	MLIE	SSIM
Original image f	39.92	31.22	——	1.87	——
STFE	40.01	96.49	30.49	2.01	0.97
GTFE	39.99	89.52	30.87	1.91	0.97
CLAHE	60.25	132.60	17.21	2.07	0.74
SSR	61.66	128.00	17.75	2.08	0.75
MSR	78.88	109.61	14.88	2.01	0.77
DGR	94.32	82.35	13.30	1.85	0.70
CLAHE-DWT	110.58	116.93	10.58	2.22	0.52
Target algorithm	78.08	117.06	14.87	2.24	0.65

Table 3 Evaluation indicator values of enhanced images under uneven lighting

Evaluation index	Mean	MLMSE	PSNR	MLIE	SSIM
Original image f	11.17	10.68	——	0.85	——
STFE	11.12	23.94	37.39	0.83	0.99
GTFE	11.12	22.51	37.74	0.75	0.99
CLAHE	23.66	23.75	23.00	0.90	0.71
SSR	20.75	18.44	24.26	0.82	0.77
MSR	44.90	34.60	16.52	1.05	0.33
DGR	49.55	12.38	16.23	0.87	0.41
CLAHE-DWT	62.71	22.52	13.32	0.90	0.28
Target algorithm	27.53	24.89	20.91	1.10	0.61

According to the objective evaluation indicators in Tables 1 - 3, the comprehensive indicator method (as shown in Eq.(14)) is used to calculate the comprehensive performance evaluation indicator F of Mean, MLMSE, PSNR, MLIE, and SSIM of the proposed algorithm and the other seven algorithms. Assuming that the PSNR and SSIM of the original image f are 1, then F is shown in Table 4.

$$F=\sum_{i=1}^{p} w_i \frac{x_i - x_{\min}}{x_{\max} - x_{\min}} \tag{14}$$

where $x_{\max}$ is the maximum value among 5 indicators; $x_{\min}$ is the minimum value among 5 indicators; x_i is the i-th indicator value of a certain algorithm; p is the number of evaluation indicators, p=5. w is the weight. The indicators of Mean, MLMSE, and MLIE in the paper are independent of each other, and w=0.25. Meanwhile, the indicators of PSNR and SSIM are highly correlated, and w=0.125.

Table 4 Comprehensive performance evaluation indicator of different algorithms

Different algorithms	Original image f	STFE	GTFE	CLAHE	SSR	MSR	DGR	CLAHE -DWT	Target algorithm
Experiment 1	0.14	0.53	0.49	0.58	0.56	0.55	0.45	0.65	0.69
Experiment 2	0.14	0.50	0.42	0.59	0.59	0.56	0.42	0.74	0.69
Experiment 3	0.20	0.44	0.37	0.45	0.34	0.69	0.36	0.52	0.60
Mean value	0.16	0.49	0.43	0.54	0.50	0.60	0.41	0.64	0.66

According to the comprehensive performance evaluation data under the three experimental conditions in Table 4, a line graph of the comprehensive performance evaluation indicator of the proposed algorithm and the other seven algorithms is drawn, as shown in Fig.6.

Fig.6 Line chart of comprehensive performance evaluation indicators for different algorithms

According to the comprehensive evaluation data, graphs, and tables of Experiment 1, Experiment 2, and Experiment 3 in Table 4 and Fig. 6, it can be seen that under 3 different experimental conditions, compared with other 7 algorithms, the comprehensive performance evaluation indicator of the proposed algorithm tends to be more stable, and the robustness is also stronger. In a low-illumination environment, the MSR has a higher comprehensive performance indicator than the proposed algorithm, but in a dust & spray, uneven lighting environment, the proposed algorithm has a better comprehensive performance indicator than the MSR, which verifies that the MSR is only suitable for light uniform environment. In the dust & spray environment, the CLAHE-DWT algorithm has a higher comprehensive performance indicator than the proposed algorithm, but in a low illumination and uneven lighting environment, the proposed algorithm has a better comprehensive performance indicator than the CLAHE-DWT. The CLAHE has a significant effect on the brightness enhancement of low-light images, and the DWT has the best effect on image noise suppression.

According to the average value of the comprehensive evaluation indicator in Table 4, draw the line graph, calculate the relative percentage of the proposed algorithm compared with the other seven algorithms, and draw the histogram corresponding to the relative percentage, as shown in Fig.7.

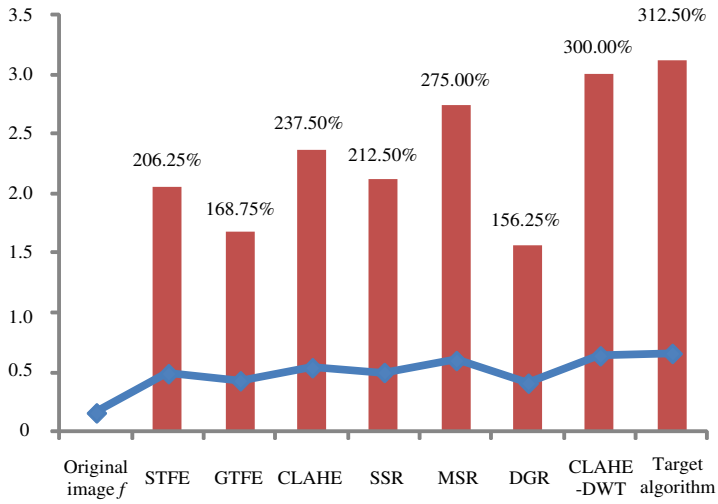

Fig.7 The average value of the comprehensive performance evaluation indicator of different algorithms and the relative percentage increase compared with the original image

According to Table 4 and Fig.7, under 3 different experimental conditions, the enhanced image of STFE, GTFE, CLAHE, SSR, MSR, DGR, MSWT and the proposed algorithm is compared with the original image, and its comprehensive performance evaluation indicator is improved respectively percentages are 206.25%, 168.7%, 237.50%, 212.50%, 275.00%, 156.25%, 300.00%, and 312.50%. Compared with the algorithm of STFE, GTFE, CLAHE, SSR, MSR, DGR, MSWT, the overall performance indicator of the proposed algorithm is improved by 34.69%, 53.49%, 22.22%, 32.00%, 10.00%, 60.98%, 3.13%, respectively. In different experimental conditions, compared with the other seven algorithms, the comprehensive performance evaluation indicator of the proposed algorithm is better, that is, the proposed algorithm has the best comprehensive enhancement performance and robustness, and is more suitable for image enhancement in different environments under mine.

5. Conclusions

The illumination environment in coal mines is complex, such as low illumination, dust & spray, and uneven lighting, etc.. These factors will lead to poor visual effects of mine images, and are not conducive to the analysis and processing of the images of Surveillance videos. In order to meet the practical application in coal mines, the paper proposes an image enhancement algorithm of degraded image enhancement using dual-domain-adaptive wavelet and improved fuzzy transform. A Garrate threshold function with adaptive adjustment factor and enhancement coefficient is designed, and an improved PAL fuzzy enhancement algorithm is constructed. Meanwhile, combining the advantages of DDF, CLAHE, gamma, Bayesian estimation and other methods in image enhancement applications, the realization principle of the proposed algorithm is established, and the block diagram of the algorithm realization principle is drawn. Finally, the de-noising and enhancement effects of the proposed algorithm in different environments of the mine are analyzed, and subjective and objective comparison and analysis are carried out with other algorithms.

The results show that the proposed algorithm can improve the overall brightness and contrast of the image, reduce the noise in the image, make the edge and detail information clearer, and the visual effect is better than other algorithms. Compared with the original image, the comprehensive performance evaluation indexes of STFE, GTFE, CLAHE, SSR, MSR, DGR, MSWT and the proposed algorithm have increased by 206.25%, 168.7%, 237.50%, 212.50%, 275.00%, 156.25%, 300.00%, 312.50%, respectively. Compared with the algorithm of STFE, GTFE, CLAHE, SSR, MSR, DGR, MSWT, the comprehensive performance index of the proposed algorithm has increased by 34.69%, 53.49%, 22.22%, 32.00%, 10.00%, 60.98%, 3.13%, respectively. Under different experimental conditions, the comprehensive enhancement performance of the proposed algorithm is the best, the robustness is the best, and it is more suitable for image enhancement in different environments in underground mines.

Data Availability

The data used to support the findings of this study are available from the corresponding author upon request.

Conflicts of Interest

The authors declare no conflict of interest

Funding Statement

This research was funded by the National Key Research & Development Program of

China (grant number 2016YFC0801800) and the National Key Research & Development Program of China (grant number 2017YFC0804300).

References

Sun JP (2010) Technologies of monitoring and communication in the coal mine. Journal of China Coal Society, 35(11): 1925-1929.

Wang GF, Liu F, Pang YH, et al (2019) Coal mine intellectualization: The core technology of high quality development. Journal of China Coal Society, 44(2): 349-357

Xu ZQ, Lv ZQ, Wang, WD, et al (2020) Machine vision recognition method and optimization for intelligent separation of coal and gangue. Journal of China Coal Society, 45(6): 2207-2216.

Zhang F, Sun XH, Cui D.L. (2018) Method of tracking and positioning for mobile target based on ORB features and binocular vision in mine. Journal of China Coal Society, 43(S2): 654-662.

Zhang W, Zhang GY (2018) Image feature matching based on semantic fusion description and spatial consistency. Symmetry, 10(12): 725.

Han H, Wang PF, Liu RH, et al (2020) Experimental study on atomization characteristics and dust-reduction performance of four common types of pressure nozzles in underground coal mines. International Journal of Coal Science & Technology. https://doi.org/10.1007/s40789-020-00329-w

Zhi N, Mao SJ, Li M (2017) Enhancement algorithm based on illumination adjustment for non-uniform illuminance video images in coal mine. Journal of China Coal Society, 42(8): 2190-2197.

Si L, Wang ZB, Xu RX, et al (2017) Image enhancement for surveillance video of coal mining face based on single-scale retinex algorithm combined with bilateral filtering. Symmetry, 9(6): 93.

Wang DW, Han PF, Fan JL, et al (2018) Multispectral image enhancement based on illuminance-reflection imaging model and morphology operation. Acta Physica Sinica, 67(21): 104-114.

Hu K, Liu S, Zhang Y, et al (2020) Automatic segmentation of dermoscopy images using saliency combined with adaptive thresholding based on wavelet transform. Multimedia Tools and Applications, 79(21): 14625-14642.

Juneja S, Anand R (2018) Contrast Enhancement of an Image by DWT-SVD and DCT-SVD. Advances in Intelligent Systems and Computing, 1 June 2017; S. Satapathy, V. Bhateja, K. Raju, B. Janakiramaiah; Data Engineering and Intelligent Computing, Springer, Singapore, pp. 595-603.

Kallel F, Hamida AB. (2017) A new adaptive gamma correction based algorithm using DWT-SVD for non-contrast CT image enhancement. IEEE Transactions on Nanobioscience, 16(8): 666-675.

Zhou M, Jin K, Wang, SZ, et al (2018) Color retinal image enhancement based on luminosity and contrast adjustment. IEEE Transactions on Biomedical Engineering, 65(3), 521-527.

Singh H, Kumar, A, Balyan LK, et al (2018) Swarm intelligence optimized piecewise gamma corrected histogram equalization for dark image enhancement. Computers and Electrical Engineering, 70(8): 462-475.

Karan SK, Samadder SR (2018) Improving accuracy of long-term land-use change in coal mining areas using wavelets and Support Vector Machines. International Journal of Remote Sensing: 39(1), 84-100.

Yang CC, Zhang MF, Zhang ZJ, et al (2018) Non-rigid point set registration via global and local constraints. Multimedia Tools and Applications, 77(24): 31607-31625.

Bae C, Chung YY, Lee J (2017) Image based video querying algorithm using 3-level Haar wavelet transform features. In 8th International Conference on Computer Science and its Applications (CSA), Bangkok, THAILAND, 19-21 December 2016; Springer Singapore, pp. 779-785.

Lei S, Lu MM, Lin JQ, et al (2020) Remote sensing image denoising based on improved semi-soft threshold. Signal, Image and Video Processing. https://doi.org/10.1007/s11760-020-01722-3.

Vishwakarma A, Bhuyan MK, Iwahori Y (2018) Non-subsampled shearlet transform-based image fusion using modified weighted saliency and local difference. Multimedia Tools and Applications, 77(24): 32013-32040.

Zhang LX, Wang YL, Deng XY, et al (2018) Wavelet Semi-soft threshold denoising based on ensemble empirical mode decomposition. Journal of Detection & Control, 40(5): 53-57.

Il KK, Hwan RU, Pil CB, et al (2017) An appropriate thresholding method of wavelet denoising for dropping ambient noise. International Journal of Wavelets, Multiresolution and Information Processing, 16(3): 1850012.

He F, He X.S. (2019) A continuous differentiable wavelet shrinkage function for economic data denoising. Computational Economics, 54(2): 729-761.

Saravani S, Shad R, Ghaemi M (2018) Iterative adaptive despeckling SAR image using anisotropic diffusion filter and Bayesian estimation denoising in wavelet domain. Multimedia Tools and Applications, 77(23): 31469-31486.

Sha YY, Xi LX, Zhang, XG, et al (2018) Application of wavelet threshold denoising in PMD measurement by fixed analyzer method," in 10th International Conference on Information Optics and Photonics, Beijing, CHINA, 8-11 July 2018; SPIE USA, pp. 109644S.

Chetih N, Messali Z, Serir A, et al (2017) Robust fuzzy c-means clustering algorithm using non-parametric Bayesian estimation in wavelet transform domain for noisy MR brain image segmentation. Iet Image Processing, 12(5): 652-660.

Sachin DR, Dharmpal, DD (2012) Image denoising with modified wavelets feature restoration. International Journal of Computer Science Issues, 9(2): 403-412.

Tang P, Guo BP (2017) Wavelet denoising based on modified threshold function optimization method. Journal of Signal Processing, 33(1): 102-110.

Zhuang LY, Guan YP (2019) Image enhancement using modified histogram and log-exp transformation. Symmetry, 11(8): 1062.

Fan WQ, and Liu Y (2020) Fuzzy enhancement algorithm of coal mine degradation image based on adaptive wavelet transform. Journal of China Coal Society. https://doi.org/10.13225/j.cnki.jccs.2020.0785.

Sun HD (2014) Wavelet core selection to mine monitoring image denosing algorithm. Coal Mine Machinery, 35(11): 271-272.

Zotin A (2018) Fast algorithm of image enhancement based on multi-scale retinex. Procedia Computer Science, 131(4): 6–14.

Zhi N, Mao SJ, Li M (2018) An enhancement algorithm for coal mine low illumination images based on bi-gamma function. Journal of Liaoning Technical University (Natural Science), 37(1): 191-197.

Huang LD, Zhao, W, Wang, J, et al. (2015) Combination of contrast limited adaptive histogram equalisation and

discrete wavelet transform for image enhancement. Iet Image Processing, 9(10): 908-915.

Kaur A, Singh, C. (2017) Contrast enhancement for cephalometric images using wavelet-based modified adaptive histogram equalization. Applied Soft Computing, 51(2): 180-191.

Figures

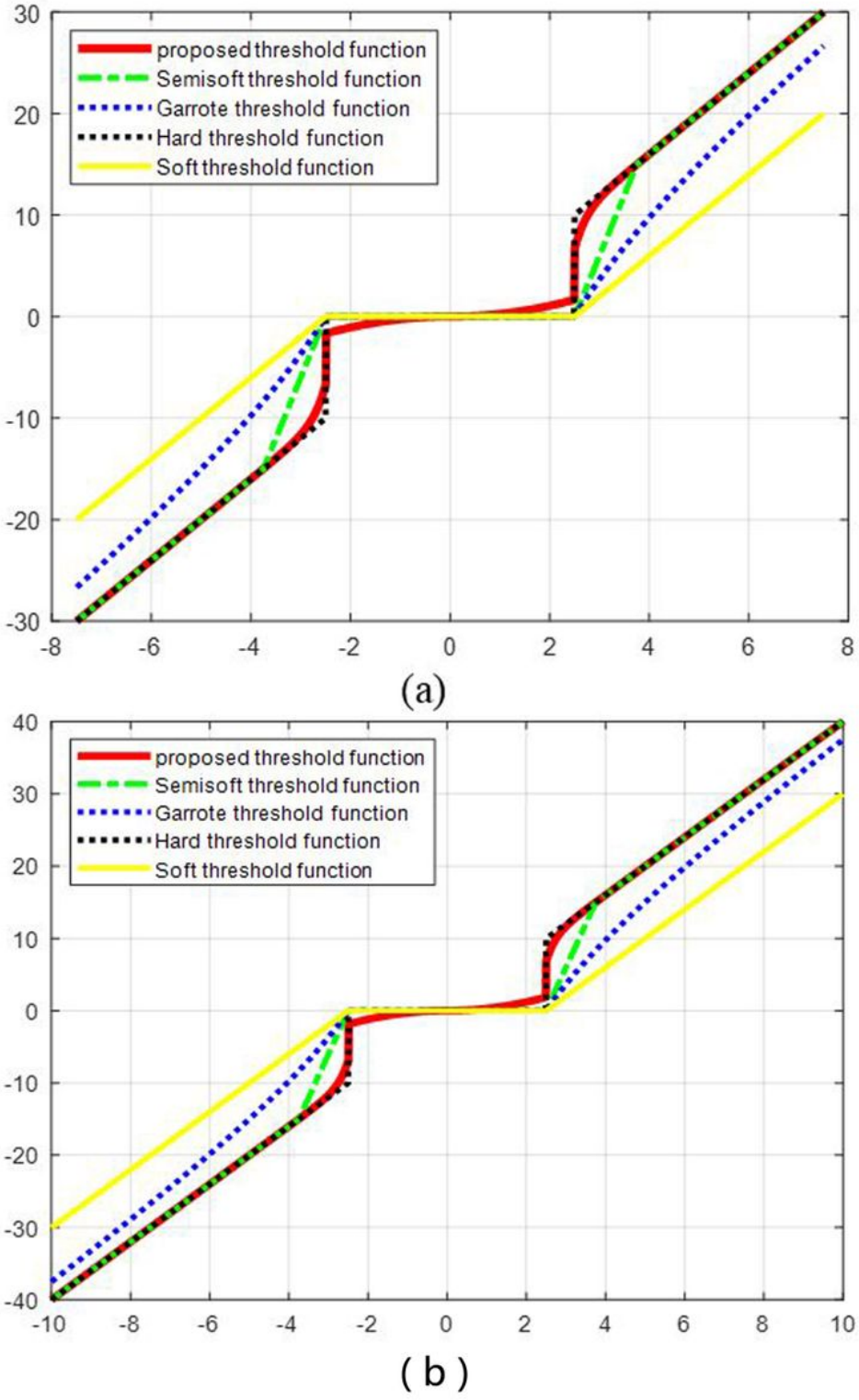

Figure 1

The proposed threshold function

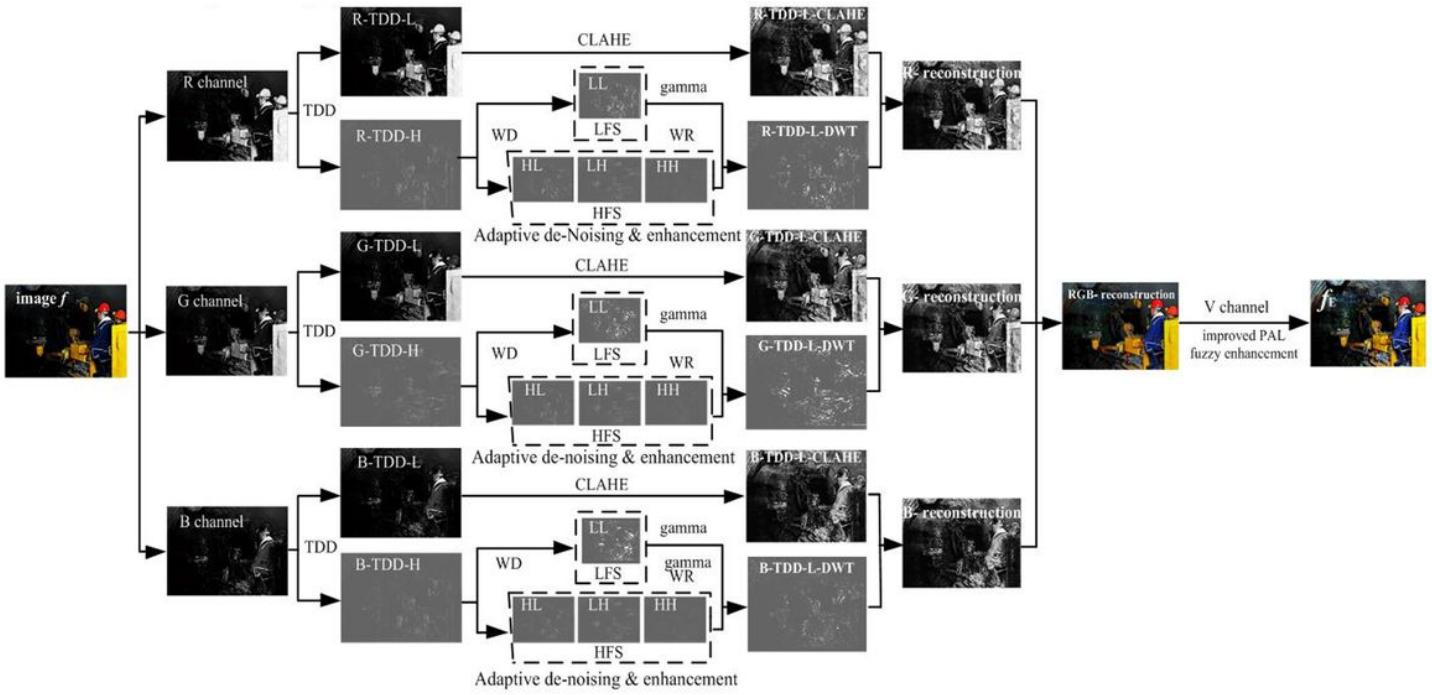

Figure 2

Block diagram of the proposed algorithm implementation principle

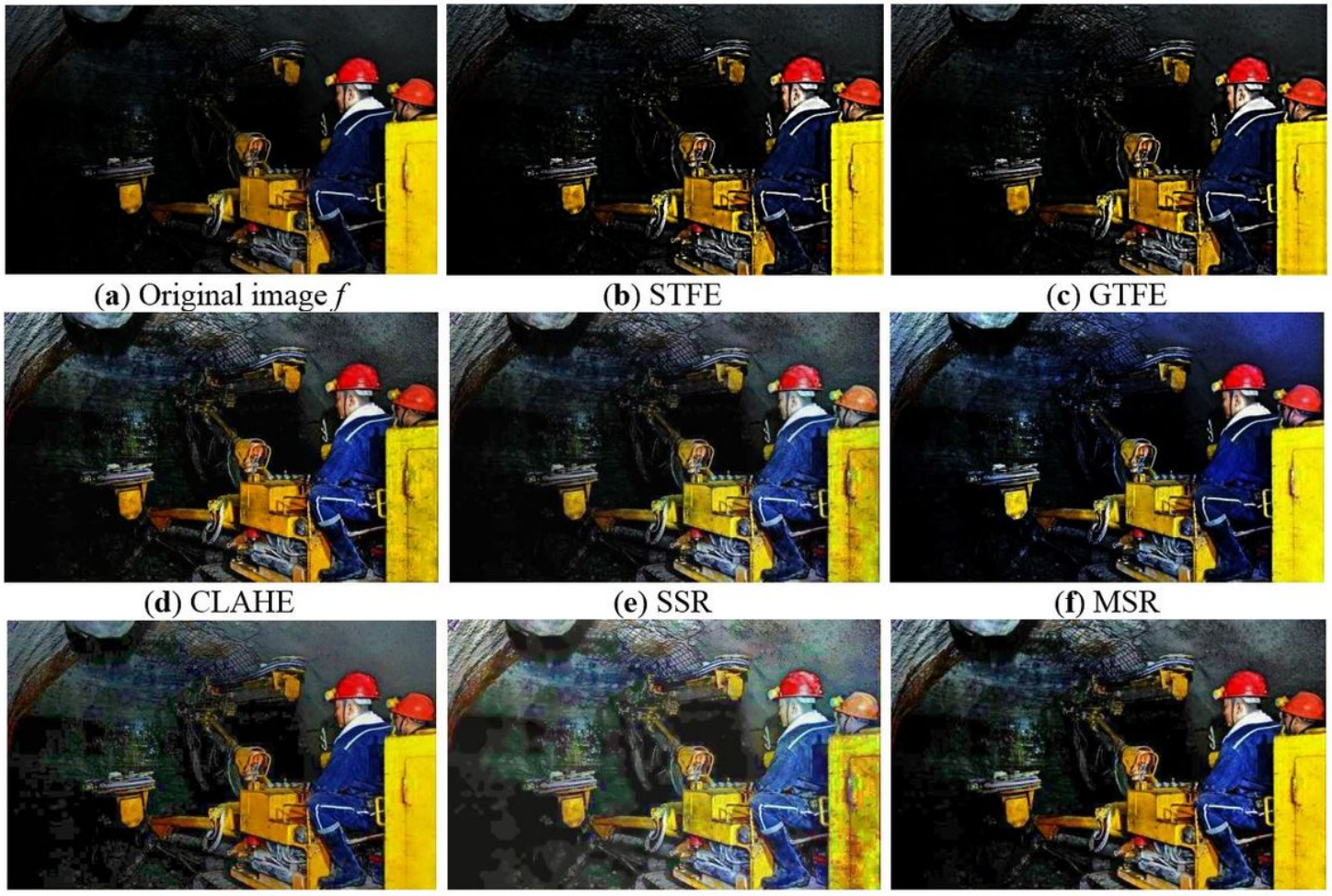

Figure 3

Low illumination image enhancement comparison chart

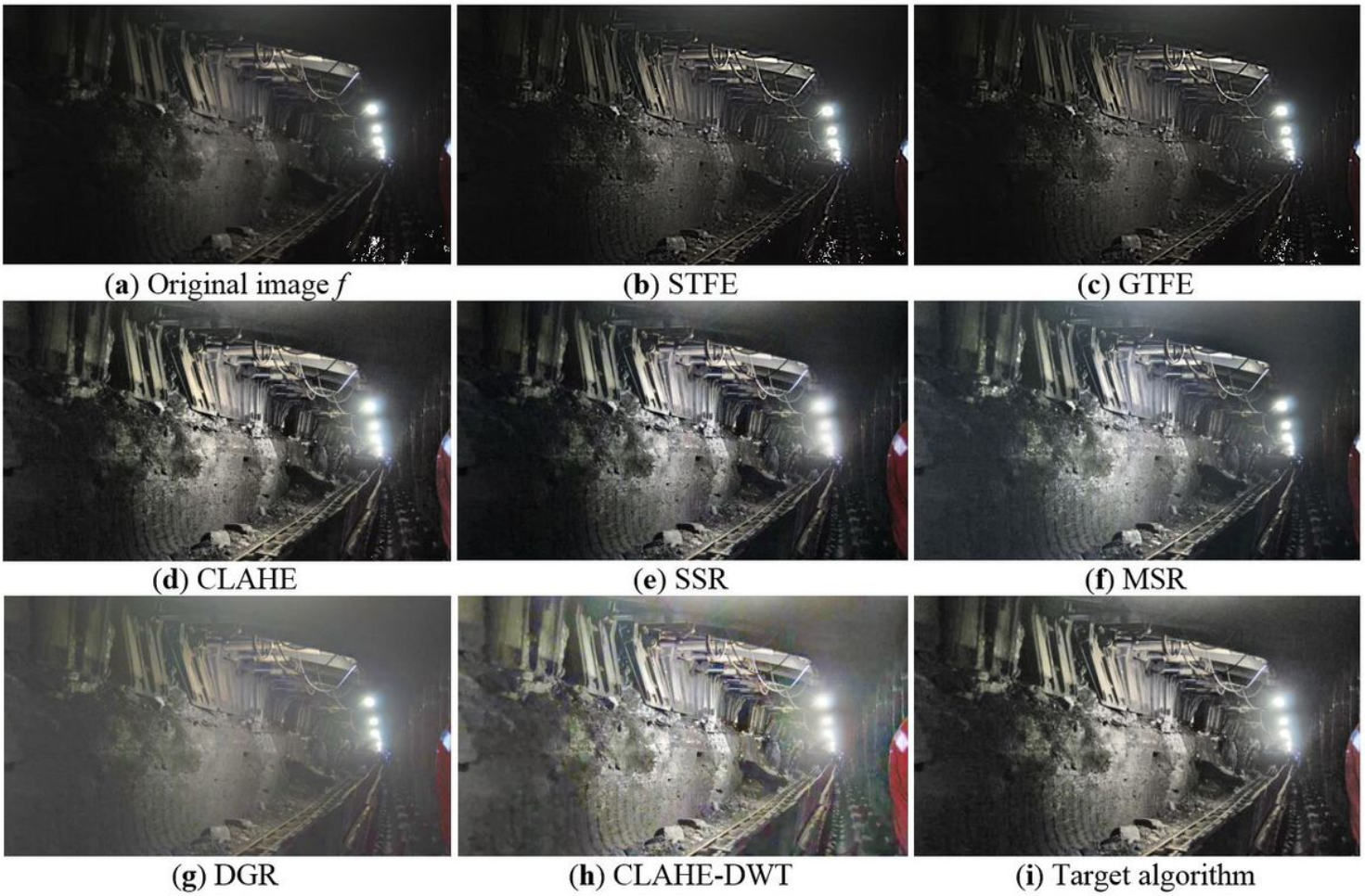

Figure 4

Dust & spray image enhancement comparison chart

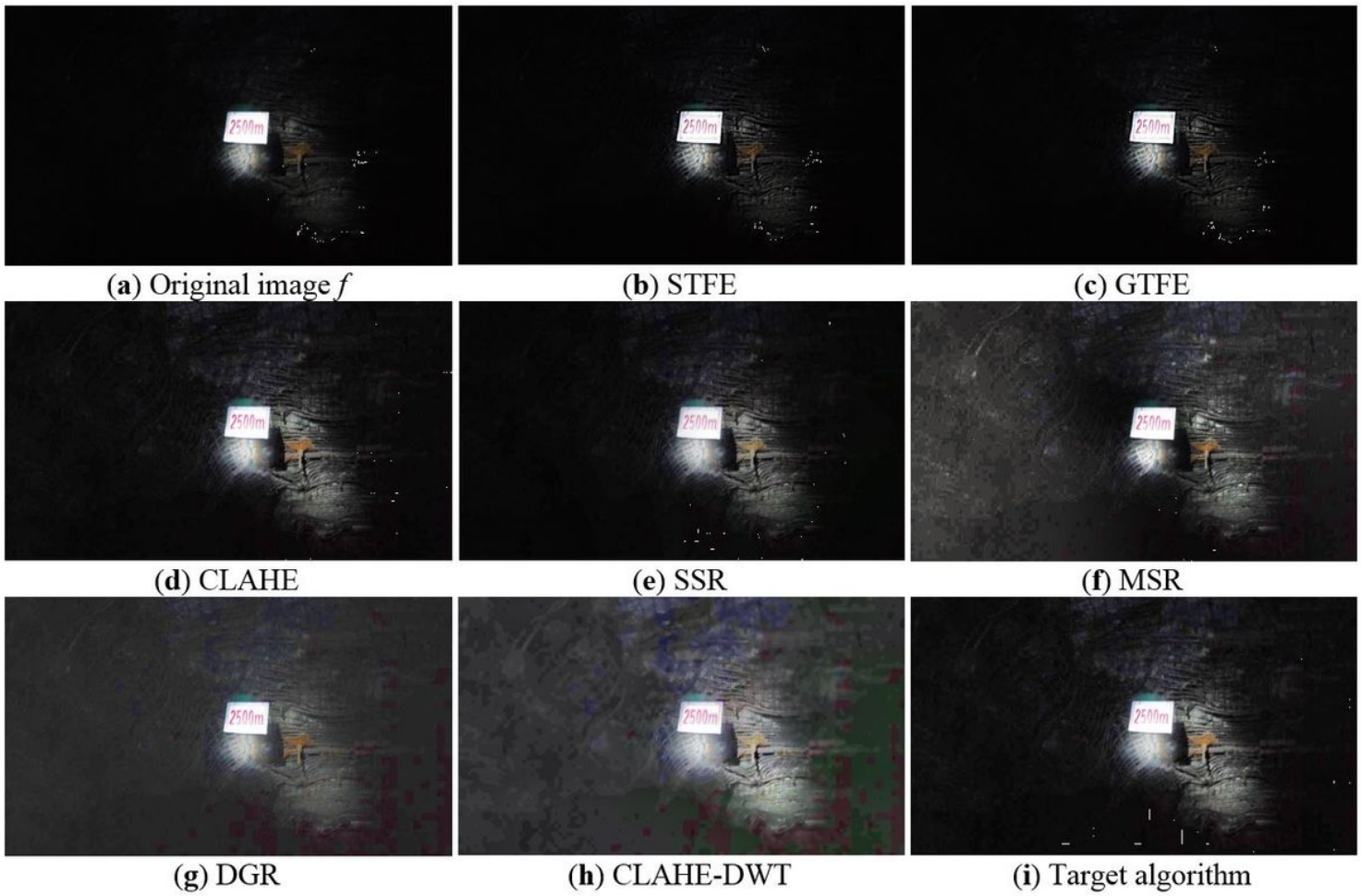

Figure 5

Uneven lighting image enhancement comparison chart

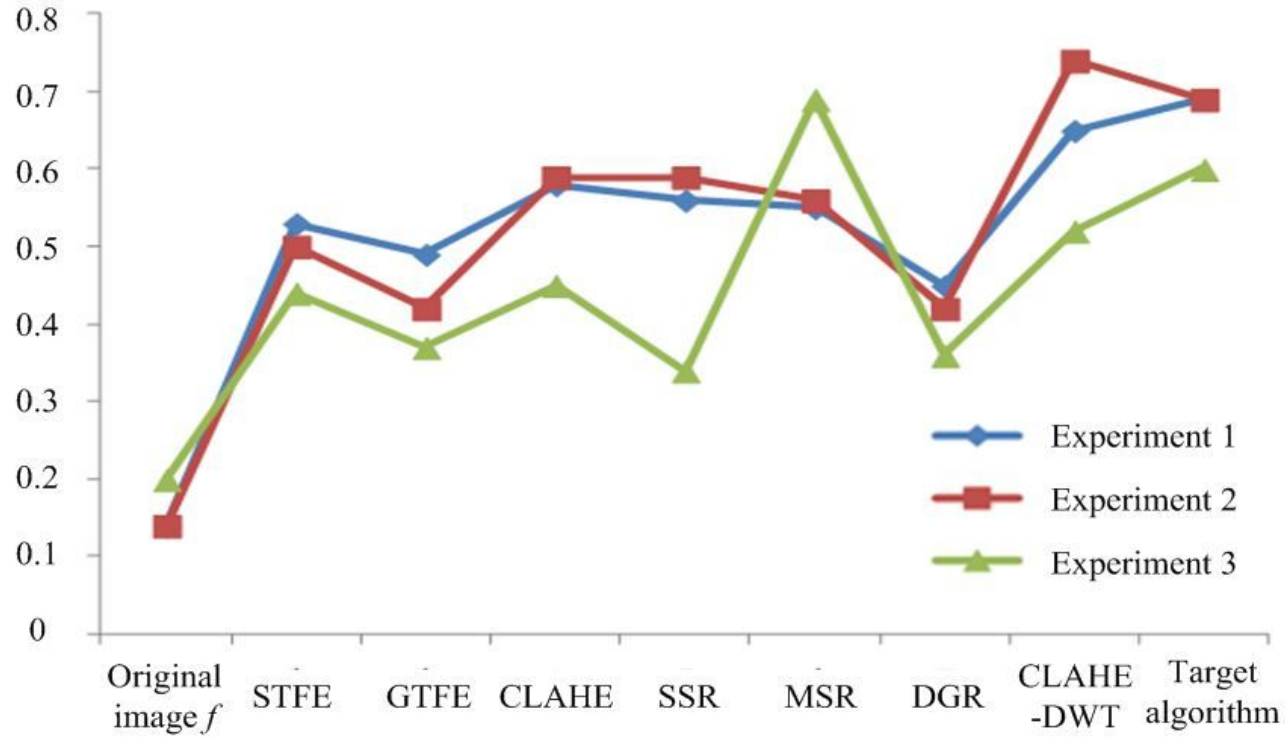

Figure 6

Line chart of comprehensive performance evaluation indicators for different algorithms

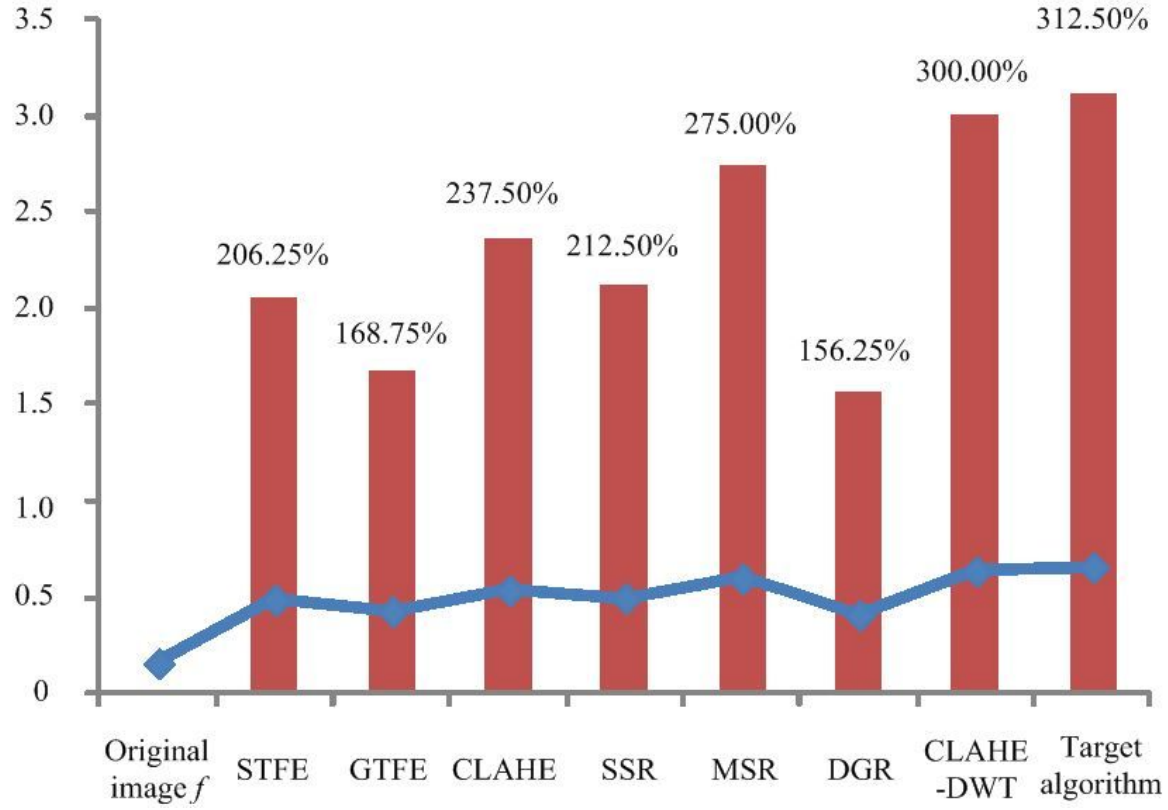

Figure 7

The average value of the comprehensive performance evaluation indicator of different algorithms and the relative percentage increase compared with the original image